Atmos. Chem. Phys. Discuss., 15, 29403–29453, 2015
www.atmos-chem-phys-discuss.net/15/29403/2015/
doi:10.5194/acpd-15-29403-2015

Atmospheric Chemistry and Physics Discussions

Exploring the variability of aerosol particle composition in the Arctic: a study from the springtime ACCACIA campaign

G. Young[1,*], H. M. Jones[1], E. Darbyshire[1], K. J. Baustian[2], J. B. McQuaid[2], K. N. Bower[1], P. J. Connolly[1], M. W. Gallagher[1], and T. W. Choularton[1]

[1]Centre for Atmospheric Science, University of Manchester, Manchester, UK
[2]School of Earth and Environment, University of Leeds, Leeds, UK
[*] *Invited contribution by G. Young, recipient of the EGU Young Scientists Outstanding Poster Paper Award 2015.*

Received: 9 October 2015 – Accepted: 13 October 2015 – Published: 29 October 2015

Correspondence to: G. Young (gillian.young@manchester.ac.uk)

Published by Copernicus Publications on behalf of the European Geosciences Union.

Abstract

Single-particle compositional analysis of filter samples collected on-board the FAAM BAe-146 aircraft is presented for six flights during the springtime Aerosol-Cloud Coupling and Climate Interactions in the Arctic (ACCACIA) campaign (March–April 2013). Scanning electron microscopy was utilised to derive size distributions and size-segregated particle compositions. These data were compared to corresponding data from wing-mounted optical particle counters and reasonable agreement between the calculated number size distributions was found. Significant variability in composition was observed, with differing external and internal mixing identified, between air mass trajectory cases based on HYSPLIT analyses. Dominant particle classes were silicate-based dusts and sea salts, with particles notably rich in K and Ca detected in one case. Source regions varied from the Arctic Ocean and Greenland through to northern Russia and the European continent. Good agreement between the back trajectories was mirrored by comparable compositional trends between samples. Silicate dusts were identified in all cases, and the elemental composition of the dust was consistent for all samples except one. It is hypothesised that long-range, high-altitude transport was primarily responsible for this dust, with likely sources including the Asian arid regions.

1 Introduction

The response of the Arctic environment to the changing climate has received increased interest in recent years due to the visible loss in sea-ice volume over the past three decades (e.g. Serreze et al., 2007; Perovich et al., 2008). The polar regions of our planet have a unique response to a warming atmosphere due to environmental characteristics vastly different to the mid-latitudes, including high surface albedo and strong variability in annual solar radiation. These factors cause the Arctic to respond to climatic changes at a heightened pace (Curry et al., 1996). The complexity of the Arctic environment requires detailed observations to further our understanding of the feed-

ACPD
15, 29403–29453, 2015

backs and underlying processes involved; however, the ability to carry out such studies is hampered by the remote location which is difficult for in-situ investigation.

Existing numerical models do not effectively reproduce the changing Arctic environment. Discrepancies in forecasted sea-ice coverage, and predicted dates for 100 % loss, are due to a variety of uncertainties within the models themselves (e.g. de Boer et al., 2014). A key uncertainty in our ability to climatologically model how these changes will progress is in our representation of atmospheric aerosol-cloud interactions (IPCC AR5, 2013). Aerosols play an important role in the Arctic radiative balance, and their influence is thought to be amplified by the unique environmental conditions of this region (Quinn et al., 2007). The annual cycle of aerosol concentration in the Arctic varies significantly by season – with highs in spring of approximately 4–5 times that observed in late summer (Heintzenberg et al., 1986) – and such variability impacts the microphysics of the mixed-phase clouds commonly observed (Verlinde et al., 2007).

The interaction of aerosol particles with clouds as Ice Nucleating Particles (INPs) or Cloud Condensation Nuclei (CCN) is dependent upon properties such as their size, hygroscopicity and composition (Pruppacher and Klett, 1997). The ability of aerosol to contribute towards microphysical structure via these pathways can have a net influence on factors such as the cloud optical depth, ice crystal/droplet number or droplet effective radius (Zhao et al., 2012); properties which can significantly affect the net radiative impact of the cloud (Curry et al., 1996). The study of INPs has developed significantly in recent years via laboratory and field studies (DeMott et al., 2010; Hoose and Möhler, 2012). It is still not clear which properties of aerosol particles promote them to act as INPs in the atmosphere. They are generally thought to be insoluble; super-micron in size; have a similar molecular structure to ice (Pruppacher and Klett, 1997); and have the potential to produce chemical bonds with ice molecules at their surface (Murray et al., 2012). For example, mineral dusts are known INPs and are used regularly in laboratory studies of ice nucleation (e.g. Zimmermann et al., 2008; Connolly et al., 2009; Kanji et al., 2013; Yakobi-Hancock et al., 2013). Sources of these particles are

ACPD
15, 29403–29453, 2015

not ubiquitous across the globe and it is not well understood which particles – and from which sources – facilitate ice nucleation in the Arctic atmosphere.

Previous studies of Arctic aerosol have indicated that the population is primarily composed of organic material, continental pollutants and locally-sourced species such as sea salt (Behrenfeldt et al., 2008; Geng et al., 2010; Weinbruch et al., 2012). There are a wide range of sources which may contribute to this population and it is difficult to quantify the impact of different regions. Some year-round studies of Arctic aerosol have been conducted (Ström et al., 2003; Weinbruch et al., 2012) which consider the differences in particle properties between seasons, showing that the annual cycle of aerosol composition and concentration is dominated by the influence of the Arctic Haze (Barrie, 1986; Shaw, 1995). Between February and April, an influx of aerosol from anthropogenic sources becomes trapped in the stable Arctic atmosphere and persists for long periods of time (up to several weeks) before being removed by precipitation processes (Shaw, 1995). During this time, the particle concentrations reach a plateau and the aerosols have the potential to interact with other species, grow and develop with a low chance of being removed from the atmosphere. This promotes an enhanced state of mixing, which compounds the difficulty in understanding how these particles interact with the clouds in the region. It is thought that the European continent is the primary source of this aerosol, with only small contributions from North America and Asia (Rahn, 1981); however, long-range transport from the Asian continent has been found to sporadically contribute to this phenomenon (Liu et al., 2015). In addition to the pollutants (e.g. as sulphate or nitrate gases), some crustal minerals have been identified in these haze events (Barrie, 1986). Improving our understanding of the properties of these particles will help us to comprehend how they influence the clouds of the Arctic, and a strong method of achieving this is by identifying the chemical composition of the aerosol particles present in the region (Andreae and Rosenfeld, 2008).

The influence of aerosol-cloud interactions on cloud microphysical structure and the Arctic radiative budget is uncertain (Vihma et al., 2014). By improving our knowledge of these processes via in-situ observational studies in the Arctic, it is possible to reduce

ACPD
15, 29403–29453, 2015

this uncertainty and develop models to produce a more accurate representation of the region's response to anthropogenic climate change. To this end, the Aerosol-Cloud Coupling and Climate Interactions in the Arctic (ACCACIA) campaign was carried out in the European Arctic in 2013, utilising airborne- and ship-based measurements to collect a detailed dataset of the Arctic atmosphere. The campaign was split into spring and summer segments, completed in Mar-Apr and July of 2013 respectively. During the spring section of the campaign, the FAAM BAe-146 atmospheric research aircraft was flown in the vicinity of Svalbard, Norway, with the capability of collecting in-situ samples of aerosol particles on filters. This study presents the analysis of the filter samples collected during this campaign, with a focus placed upon identifying the compositional properties and sources of the non-volatile, coarse-mode aerosol particles present in the atmosphere during the Arctic spring.

1.1 Campaign overview

The flights of the springtime ACCACIA campaign were mainly conducted in the region to the south-east of Svalbard, with the exception of flight B768 which was carried out to the north-west near the boundary with Greenland. Figure 1 details the science sections of each of the springtime flights of interest, with direction from Svalbard to Kiruna, Sweden in all cases except B765, and the corresponding dates are listed in Table 1. For the majority of these flights, a focus was placed on obtaining atmospheric measurements over the marginal ice zone between the sea-ice and the ocean, allowing the variation of cloud structure with surface conditions to be investigated.

As part of the springtime campaign, 47mm-diameter Nuclepore polycarbonate filters were exposed on-board the FAAM BAe-146 aircraft to collect in-situ samples of the accumulation- and coarse-mode aerosol particles (sizes $\sim 0.1\,\mu m$ to $\sim 10\,\mu m$). Such particle sizes are approximately applicable to the study of CCN and INPs (Pruppacher and Klett, 1997). This study presents the analysis of one set of filters from each of the flights shown in Fig. 1, placed in the context of how the characterised particles may interact with the cloud microphysics in the region.

ACPD
15, 29403–29453, 2015

2 Methodology

2.1 Aircraft instrumentation and trajectory analysis

During the spring section of the ACCACIA campaign, a range of cloud microphysics and aerosol instrumentation were used on board the FAAM BAe-146 aircraft to produce a detailed record of the observed Arctic atmosphere (as described by Liu et al., 2015; Lloyd et al., 2015). In this study, data from the Cloud Droplet Probe (CDP-100 Version 2, Droplet Measurement Technologies (DMT), Lance et al., 2010), the Cloud Aerosol Spectrometer with Depolarisation (CAS-DPOL, DMT, Glen and Brooks, 2013) and the Passive Cavity Aerosol Spectrometer Probe (PCASP 100-X, DMT, Rosenberg et al., 2012) are used to provide context for and a comparison to the filter measurements.

The accumulation-mode aerosol distribution was monitored by the PCASP, whereas the CAS-DPOL measured both coarse-mode aerosol and, along with the CDP, cloud droplet number concentration. These externally-mounted aircraft probes size and count their relative species via forward-scattering of the incident laser light through angles 35–120° and ∼4–12° (for both the CDP and CAS-DPOL) respectively. The PCASP measures particle concentrations and sizes in the range of 0.1 to 3 µm, the CAS-DPOL provides similar measurements from 0.6 to 50 µm (Glen and Brooks, 2013), and the CDP measures cloud droplets from 3 to 50 µm (Rosenberg et al., 2012).

Out of cloud, the CDP and may be used to provide an indication of the wet-mode diameter of coarse-mode ambient aerosol particles. The CAS-DPOL also measures coarse-mode aerosol concentrations when out of cloud. Within cloud, the liquid-water content (LWC) can be derived from the observations of cloud droplet size. In this study, a LWC threshold of $\leq 0.01\ \mathrm{g\,m^{-3}}$, derived from CDP measurements, was employed to distinguish between out-of-cloud and in-cloud measurements, and this threshold was applied to the CAS-DPOL, CDP and PCASP data to obtain an estimate of the ambient aerosol size distributions. These out-of-cloud observations are used in this study to validate the collection efficiency of the filter inlet system.

ACPD
15, 29403–29453, 2015

In addition to the in-situ data gained from the instrumentation aboard the aircraft, back trajectory analyses were carried out to further contextualise the filter exposures. This was achieved using HYSPLIT 4 (Draxler and Hess, 1998), in a similar manner to Liu et al. (2015). Horizontal and vertical wind fields were derived from GDAS reanalysis meteorology (NOAA Air Resources Laboratory, Boulder, CO, USA) and used to calculate trajectories at 30 s intervals along the FAAM BAe-146 flight path. This analysis allows the direction of the air mass to be inferred; however, it does not explicitly account for turbulent motions along the derived path and therefore carries a degree of uncertainty (Fleming et al., 2012). Trajectories dating back 6 days are presented to provide an indication of the source regions of the particles collected during the ACCACIA filter exposures.

2.2 Filter collection

The filter collection mechanism on the FAAM BAe-146 aircraft comprises a stacked-filter unit (SFU) which allows for two filters to be exposed simultaneously to the air stream, allowing aerosol particles to be collected on both. In the ACCACIA campaign, a combination of two filters with different nominal pore sizes was used in each exposure – a 10 µm-pore filter was stacked in front of a 1 µm-pore filter – allowing sub-micron aerosol particles that may pass through the pores of the first to be collected by the second. This mechanism allows for the approximate splitting of the total aerosol size distribution onto two filters.

The design of the inlet follows the same specifications as the MRF C-130 aircraft filtration system described extensively by Andreae et al. (2000) and allows for sub-isokinetic sampling, thus removing large cloud droplets from the sampled air and minimising any particulate contamination from cloud droplets or rain (Chou et al., 2008; Johnson et al., 2012). Due to this design, large particles (>10 µm) are also thought to be removed from the collected sample, though the collection efficiency of the entire system is not known to have been formally quantified (Formenti et al., 2008; Johnson et al., 2012). Despite this, the efficiencies of the filters themselves can be estimated:

ACPD
15, 29403–29453, 2015

the 50 % cut-off diameter of the 10 µm Nuclepore filter is approximately 0.8–1 µm at the mean face velocity encountered during this study (~ 100 cm s^{-1}) (John et al., 1983; Crosier et al., 2007), whilst the 1 µm filter has a 50 % collection efficiency at approximately 0.2 µm (Liu and Lee, 1976). Qualitatively, this sampling method has been found to compare reasonably well with wing-mounted particle counters (Chou et al., 2008; Johnson et al., 2012).

The filters were typically exposed on straight, level runs for approximately 10–30 min to obtain a sufficient sample for chemically-speciated mass loadings. Although the filter system was designed to remove cloud droplets, the filters were primarily exposed out of cloud to further minimise the potential for contamination. Chosen filters were all exposed within the boundary layer (< 1000 m, see Tables 2 and 5) with no dependence on whether the surface was sea-ice covered or open ocean. Samples from below cloud were preferentially studied in this investigation as they likely included the main contributions of CCN and INPs at this time of year; however, one exposure from above cloud is considered in Sect. 3.4.

2.3 Environmental scanning electron microscopy

Using a Phillips FEI XL30 Environmental Scanning Electron Microscope with Field-Emission Gun (ESEM-FEG) in partnership with an Energy-Dispersive X-Ray Spectroscopy (EDS) system, automated single-particle analysis of the ACCACIA filter samples was undertaken at the University of Manchester's Williamson Research Centre (Hand et al., 2010; Johnson et al., 2012).

The coupled EDS system allows for morphological and compositional single-particle analysis. The electron beam is controlled by the EDS system to provide automated analysis of the sample and record detailed data of each particle imaged. The resultant compositional output is a relative elemental weight percentage of each measured element – summed to a total of 100 % – derived from the X-ray spectrum recorded by the EDAX™ Genesis software. To compute each elemental weight percentage, a standardless ZAF correction method was applied; corrections which relate to atomic number,

ACPD
15, 29403–29453, 2015

absorption and fluorescence respectively. The software detects particles via the intensity of the resultant image and allows the particles to be viewed under greyscale contrast with the approximately uniform composition of the background filter. The parameters chosen for this analysis are listed in Table 3 and a carbon-coating was applied to each sample to allow the analysis to be carried out using the high vacuum mode. Contributions from the following elements were measured for each particle detected: C, O, Na, Mg, Al, Si, P, S, Cl, K, Ca, Ti, Cr, Fe, Ni, Cu and Zn. The primary morphological properties computed by the EDS analysis include average diameter, shape and aspect ratio. These are derived from the particle area measured by the software, which itself is determined from the number of pixels illuminated per particle analysed. The minimum size detectable corresponds to 4 pixels in the given image.

Additionally, to act as a calibration, a blank filter was analysed as Nuclepore filters have been shown to carry contaminants themselves (Behrenfeldt et al., 2008). A small number of particles were identified, yet they appeared almost transparent under contrast and the majority produced a spectra similar to the background filter when analysed. Amongst the remaining particles, there was a notable metallic influence and some particles were found to have moderate Cr or Fe fractions. This mirrors the result presented by Behrenfeldt et al. (2008) and their presence casts doubt over the origin of particles displaying this signature in the real data cases; however, these particles were found to be few in number and so should not greatly affect the outcome of this analysis.

This technique has been applied by several studies (e.g. Kandler et al., 2007; Hand et al., 2010; Formenti et al., 2011; Weinbruch et al., 2012) to investigate the chemical composition of particles from a variety of sources. These studies have shown that there are some limitations to consider with this technique. In general, the ESEM/EDS system is capable of quantifying the weight percentage of any element of an atomic number $Z > 4$ (Beryllium) (Formenti et al., 2011). The filters used in the ACCACIA campaign are primarily composed of C and O, thus they contaminate the measurements of these elements in each particle. Previous studies which have used these polycarbonate filters have excluded precise measurements of carbon and oxygen from their analysis to

ACPD
15, 29403–29453, 2015

combat this issue (e.g. Krejci et al., 2005; Behrenfeldt et al., 2008; Hand et al., 2010). In a similar manner, only elements with $Z > 11$ (Sodium) were considered for the compositional analysis undertaken in this study.

The electron beam produced by the ESEM can negatively interact with some particle species, causing them to deform (Behrenfeldt et al., 2008). This visible deformation is caused by the evaporation of the volatile components of the particles, either under the electron beam or as a result of the high vacuum (Li et al., 2003; Krejci et al., 2005). Little can be done to prevent this and it is especially difficult to manage when applying the automated particle analysis method used in this study. Behrenfeldt et al. (2008) investigated this phenomenon and found that it only had a small impact on their results and could be disregarded. As a result, it can therefore be assumed that the particles analysed by this method are dry and that any volatile components will have evaporated (Li et al., 2003). There are also several implicit factors which may contribute some degree of uncertainty to the quantitative composition measurements gained. For example, errors can be introduced by uncertainties in the spectral fitting of the EDAX™ software (Krejci et al., 2005) or from the differing geometries of the individual particles measured (Kandler et al., 2007). Also, compositional data for particles less than 0.5 µm should be treated with caution due to increased uncertainty at smaller sizes (Kandler et al., 2011). As with the study by Kandler et al. (2007), the sample sizes considered here were too large to consider individual corrections, therefore the compositions achieved by the EDS analysis were taken as approximate values. Similarly, manual inspection of the images and spectra, as carried out by Hand et al. (2010), was not feasible due to the sample size and so an algorithm was imposed to remove any filter artefacts. These were typically a result of the software misclassifying the filter background as a particle itself and therefore displayed only the distinctive background signature. This background spectrum presented different characteristics than those considered to be carbon-based; the artefacts were noisy, with very low detections in all but a few of the elements, whereas the particles thought to be carbonaceous displayed zero counts in some elements as expected. The number of detected particles removed by this al-

ACPD
15, 29403–29453, 2015

gorithm was typically low and it is not possible to conclude if any real particles were removed. Krejci et al. (2005) placed an estimate of the total error involved with this technique to be around 10 % and found this value to be dependent on the sample and elements analysed. These approximations are acknowledged in the different analysis methods applied to the data in this study.

2.4 Classifications

Elemental information gained from EDS analysis can be taken further to identify particle species relevant to the atmosphere. These may typically include organic material, black carbon, mineral dusts and/or sea salt, dependent on the measurement location.

The classification scheme applied in this investigation was derived from a variety of sources (e.g. Krejci et al., 2005; Geng et al., 2010; Hand et al., 2010); however, it is most prominently based upon the detailed scheme presented by Kandler et al. (2011). The main criteria of this scheme are summarised in Table 4.

2.4.1 Carbonaceous and biogenic

A crucial property of the classification scheme adopted by Mamane and Noll (1985) is that they considered particles with only C and O measurements to be organic or biological in nature. This approach has been adopted by other studies which applied a polycarbonate substrate (e.g. Kandler et al., 2007; Behrenfeldt et al., 2008; Hand et al., 2010). For example, particles included in this category could be soot particles or pollen grains (Behrenfeldt et al., 2008). Mamane and Noll (1985) developed this idea to segregate between carbonaceous and biogenic as they found a high quantity of measurable coarse-mode pollen grains in their samples. These were found to be dominated by carbon and have high spectral backgrounds with distinctive small peaks in P, S, K and/or Ca. The study by Geng et al. (2010) utilises a comparable threshold to make a similar distinction; however, they also consider small amounts of Cl, S, K, N

ACPD
15, 29403–29453, 2015

and/or P as indicators as these elements are important nutrients for plant life (Steinnes et al., 2000).

The carbonaceous and biogenic classifications likely include particles that may have some volatile component which cannot be measured by this technique (see Sect. 2.3), therefore the partial or complete evaporation of these particles will consequently cause the presented fraction to be a lower-limit, i.e. only the non-volatile cases can be measured. Coupled with the difficulty of distinguishing these particles from the filter background, it is important to note that the particle fractions of the carbonaceous and biogenic classes presented by this study are approximations which are likely underestimating the true organic loading on these filters.

2.4.2 Sulphates, fresh and mixed chlorides

Sodium Chloride from sea salt (NaCl) can enter the atmosphere as a consequence of sea-surface winds and these particles remain predominantly sodium- and chlorine-based for a short period of time. The lifetime of Cl is hindered by the tendency of these particles to accumulate sulphate in the atmosphere, thus producing particles primarily composed of Na-S as identified by Hand et al. (2010). Due to the short lifetime of this Cl source in the atmosphere, its presence is often used to indicate a fresh contribution from the sea surface (Hand et al., 2010). It is a common conclusion that a lack of Cl-containing particles and/or a significant fraction of S in a particulate sample is suggestive of aged aerosol (Behrenfeldt et al., 2008; Hand et al., 2010).

These aged species can infer an anthropogenic influence in a sample, as they are thought to require a reaction with sulphur or nitrogen oxides (Geng et al., 2010). However, the Arctic ocean is a source of dimethylsulphide (DMS); a gas which can also interact in the atmosphere to form sulphur dioxide. The contribution of this source is greater during the summer months due to decreased sea-ice (Quinn et al., 2007), and therefore is thought to have little influence during the dates of this study. The gas source cannot be concluded here but it can be stated that Na-S particles will have been present in the atmosphere for a sufficient length of time to allow the interaction to

ACPD
15, 29403–29453, 2015

take place. In this study, the mixed chlorides category requires that the particles must still be predominantly Na- and Cl- based, with a notable S contribution. This category also accounts for metallic contributions to the base NaCl species. The sulphates and fresh chloride categories are limited to the extremes of this distribution, with only S- and Cl-dominated signatures allowed respectively.

2.4.3 Silicates, mixed silicates, Ca-rich and gypsum

Complex internal mixing in particles is often indicative of a natural origin (e.g. Conny and Norris, 2011; Hoose and Möhler, 2012); however, coagulated particles can also be produced by high-temperature anthropogenic activities. Studies have indicated that a strong method of sourcing internally-mixed particles could involve the identification of silicon: particles consisting of this element and various mixed metals are likely to be naturally-occurring mineral dusts, and industrial by-products may lack this element in high quantities (Conny and Norris, 2011). Mineral dusts are typically composed of a variety of elements and tend to include significant fractions of Si and Al, with more minor contributions from Na, Mg, K, Ca and/or Fe amongst others.

Dusts are crucial constituents of the aerosol population as they are proven Ice Nucleating Particles (INPs) (Zimmermann et al., 2008; Murray et al., 2012; Yakobi-Hancock et al., 2013). However, they can also act as Cloud Condensation Nuclei (CCN); Ca-based dusts have been shown to react with nitrates in the atmosphere to produce hygroscopic particles that may act as CCN (Krueger et al., 2003). The concentrations of nitrates in the Arctic during March (measured at the Alert sampling station in Canada) followed an increasing trend over 1990–2003 (Quinn et al., 2007), suggesting there is some probability that this interaction could take place in this environment. Alternatively, under specific environmental conditions, internally-mixed particles consisting of dusts, sulphates and sea salt can act as Giant CCN (Andreae and Rosenfeld, 2008). In this study, the presence of such particles may be inferred by the additional detection of S or Cl with the typical dust-like signatures. This can occur if the dust in question has been transported over long distances and thus undergone cloud processing or acidification

ACPD
15, 29403–29453, 2015

reactions (Mamane and Noll, 1985; Behrenfeldt et al., 2008). Or, more simply, these could be the result of a sea salt or sulphate coating on a mineral dust particle, and such mixtures have been modelled to have significant effects on warm clouds by augmenting the CCN population (Levin et al., 2005). Complex internal mixtures containing Si, S and/or Cl are therefore indicated in this study under the classification mixed silicates.

It is difficult to identify particular species of mineral dusts using the EDS method as these particles are closely related compositionally; there are minimal differences between the chemical formulae of some dusts and this may not be accurately detectable by the method. In several studies (e.g. Kandler et al., 2007; Hand et al., 2010), the specific phases of the mineral dusts observed were not quantified, instead they considered both the individual X-ray counts and ratios between the elements measured to classify their sampled particles into set groups such as silicates and carbonates. It has often been considered that Al, Ca and K are indicative of aluminosilicates (such as Kaolinite), carbonate minerals – such as Calcite ($CaCO_3$) and Dolomite ($CaMg(CO_3)_2$) – and clays/feldspars respectively (Formenti et al., 2011). Some mineral classes have a distinct elemental relationship and these may be easier to classify; for example, Gypsum ($CaSO_4 \cdot 2H_2O$) samples typically do not deviate from their base chemical formulae whereas others (especially amongst the aluminosilicates) can vary widely (Kandler et al., 2007). By this reasoning, Gypsum was included as its own classification, whereas the vast majority of mineral dusts observed were grouped into the silicates, mixed silicates and Ca-rich categories, dependent on the relative quantities of Si, S and Ca they contained.

2.4.4 Phosphates and metallics

These groups include particles with significant influences from phosphorus and transition metals respectively. Particles classified as phosphates in this study may include those composed of Apatite – a Ca- and P-based mineral group – as factories tailored towards processing these minerals are common in the nearby Kola Peninsula, Russia (Reimann et al., 2000).

ACPD
15, 29403–29453, 2015

The presence of transition metals in the collected particles can be viewed as an indicator for an industrial origin (Weinbruch et al., 2012). In this study, potential anthropogenic local sources for the metallic particles may be the coal burning facilities on Svalbard (in Longyearbyen and Barentsburg) or various metal smelters in the Kola Peninsula, Russia (Weinbruch et al., 2012). The metals included in the EDS analysis were Ti, Cr, Fe, Ni, Cu and Zn. Contributions from these may be attributable to anthropogenic and/or natural sources and could be in the form of metal oxides or constituents of complex minerals (Hand et al., 2010). For example, Fe can occur naturally and is common within clay minerals, but it may also be sourced from anthropogenic smelting factories and ore mines (Steinnes et al., 2000). Of those measured in this study, Fe and Al are the most likely to originate from a variety of sources as they are processed widely (Steinnes et al., 2000) and are common constituents in silicate-based dusts. Similarly, Zn may also be associated with biological material in addition to smelting emissions (Steinnes et al., 2000).

2.4.5 Biomass tracers

This group was introduced out of necessity given the results obtained. The other classifications were somewhat expected from hypothesised local sources; however, this group was introduced to account for the high quantity of potassium-based particles observed in one of the flights. These particles have negligible measurements of silicon and are not thought to be mineralogical in nature. This category has been dubbed "Biomass Tracers" as several studies (e.g. Andreae, 1983; Chou et al., 2008; Hand et al., 2010; Quennehen et al., 2012) have identified particles sourced from biomass burning events to be rich in this element. These K-rich particles have been found to be prominent in forest fire and anthropogenic combustion emissions, and may not be expected to be present in the Arctic atmosphere (Quennehen et al., 2012). Biomass burning produces particles known as bottom ashes, which differ from the fly ash particles that are typically emitted during fossil-fuel incomplete combustion processes (Umo et al., 2015). Activities which may produce these constituents could include firewood

ACPD
15, 29403–29453, 2015

or agricultural burning (Andreae, 1983), or wildfires in warmer climates (Seiler and Crutzen, 1980).

2.4.6 Other

This group contains particles which are not classified by the applied scheme. The implication is that these particles are well-mixed. Figure 2 illustrates the difficulty with internally-mixed particles; though local sites on the particle may be strongly influenced by certain elements, the automated scan will not catalogue the spatial dependencies and instead computes a mean spectra for presented particle surface area.

Internally-mixed particles are typically either unclassified or classified by their most abundant elements on average. The particle illustrated in Fig. 2 would be classified as a silicate dust since it is well-mixed but has a dominating Si influence. The size of the samples prevent manual inspection of every internally-mixed particle, therefore the abundance of well-mixed particles within a dataset must be inferred from the quantity quoted as "Other".

3 Results

3.1 HYSPLIT back trajectories

Air mass histories were calculated using HYSPLIT for each of the filter exposures to provide context with the environmental conditions in which they were sampled. Figure 3 shows the spatial extent of these trajectories in the top two panels and the mean altitudes covered are shown in the bottom panel.

The mean altitude of the trajectories remains within the lower 1.5km of the atmosphere. The modelled altitude typically increases monotonically with increased time backwards. The case from B765 is the exception to this trend, as consistent low-altitude trajectories are modelled for the full duration shown. Also, the majority of these trajec-

ACPD
15, 29403–29453, 2015

tories are reasonably smooth; however, a significant descent in height is modelled in the B764 case at approximately -2 days.

A north-easterly wind was observed for cases B760 to B762, bringing air from over the dense Arctic sea-ice to the region of interest to the south-east of Svalbard. When extended back by 6 days, it becomes apparent that the history of the air sampled in each of these cases is quite different. From Fig. 3, B760 and B761 show some similarities, with the latter displaying more curvature anti-clockwise than the former. The trajectories from the B762 exposure are markedly distinct from these two, with cyclonic curvature around the immediate vicinity of Svalbard and Greenland.

There is a clear partition in the direction of the trajectories as the spring campaign progressed. The first three exposures had source regions to the north and west of the exposure locations, whilst the latter three primarily sampled from the east. These latter trajectories also appear to be more compact than the first three cases (Fig. 3). The air from B764 and B765 is traced back across the northern coast of Russia whilst the B768 trajectories split in two and cover the northern coast, inland Siberia and Scandinavia. A large portion of these trajectories are clustered towards the continent, suggesting a strong influence on this sample from this region.

These two trajectory groups can be dissected further; two specific pairs can be identified (B760 and B761; B764 and B765) which display similar paths, and B762 and B768 appear unique in comparison. Overall, there appears to be a clear shift in the source region of these boundary layer exposures as the campaign progresses; from over the dense Arctic sea ice, through Greenland and Northern Russia to the European continent.

3.2 Aerosol size and morphology

To investigate any issues with inlet collection efficiency (see Sect. 2.2), size distributions of the resultant filter pair analysis were constructed and compared with those averaged from the wing-mounted aircraft probes. The number size distribution was computed similarly to Chou et al. (2008); namely, the total number of particles de-

ACPD
15, 29403–29453, 2015

tected in each scan was normalised by the area covered by the scan and the total volume of air sampled, then scaled to the full filter area. Figure 4 illustrates these comparisons for each below-cloud filter pair analysed. Data from the PCASP, CAS-DPOL and CDP instruments were combined to give a single distribution for each case: the CAS-DPOL data were used between sizes 2 and 10 µm, with PCASP data used below 2 µm and CDP data used above 10 µm. These data use the standard scattering cross-sections for the aircraft probes and no refractive index corrections were applied due to the expected well-mixed aerosol population.

The agreement of the filter-derived data with the probe data is clearly dependent on the conditions sampled. For example, the B762 filter pair was exposed during a section where cloud haze was encountered, whereas the B765, B768 and B760 cases were cleanly exposed out of cloud. The B761 and B764 cases appeared to sample small amounts of cloud at the end of their exposures – at which point the probes measured some amount of cloud droplets and/or swollen aerosol particles – therefore the distribution derived from the external probes differs somewhat to the filter particle distribution. Qualitatively, there is reasonable agreement between the probe and ESEM-derived number size distributions – providing confidence in the analysis presented in this study – but this similarly highlights the limitations of the sample inlets on the aircraft for coarse aerosol as described by Trembath (2013).

3.3 Aerosol composition

The particle classifications detailed in Sect. 2.4 were applied to the compositional data obtained for each analysed filter pair. An element index was introduced which takes the ratio of the weight percentages measured for each element to the sum from all elements measured (excluding C and O) for each particle, thus allowing the relationships between the elements of interest to be considered in isolation from the filter influence (Mamane and Noll, 1985; Kandler et al., 2007).

Figure 5 displays the averaged classifications for each flight, split into sizes less than and greater than 0.5 µm. There is high variability in composition between each flight.

ACPD
15, 29403–29453, 2015

The contributions of metallic and mixed chloride particles are approximately independent of size; however, some categories display a clear dependence. For example, sulphates, carbonaceous and biomass tracers are detected strongly in the sub-micron range whilst silicates and fresh chlorides dominate the super-micron range.

The dependence of composition on size is emphasised in Fig. 6, where only the sizes which show good agreement with the wing-mounted probes have been included (~ 0.5–~10 µm). Size-segregated compositional data for sizes smaller than this range have not been included as these may not be representative of the true conditions (see Fig. 4) and also have increased signal-to-noise issues from the measurement technique (Kandler et al., 2011).

Clear trends become apparent when implementing this size-segregated approach. In all samples, silicate-based dusts are identified, with greater concentrations clearly found at larger sizes for all cases except B768. The presence of these dusts is most abundant in the first three cases. Filters from B764 and B765 are heavily dominated by fresh chlorides at all sizes except the largest bins, and B762 and B768 also have significant fractions of this species. The B768 sample differs from the others, displaying increased Ca-rich, mixed chloride and other fractions. Similarly, the high sulphate loading in B760 is unlike the other cases, yet the composition trends of this case can be associated with the subsequent flight via the abundance of silicates; a link that is not so clear between B765 and B768.

With regards to the mineral phase of the silicate dusts collected, elemental ratios can be used to identify trends. For example, feldspars can be rich in Ca, K or Na, whilst clays may have significant fractions of Mg and/or Fe. The elemental ratios displayed in Fig. 7 are variable across the campaign. This variability is heightened in some ratios with respect to others; from Fig. 7, it is clear that the K/Al ratio is highly changeable but the Mg/Si ratio is low for all cases. The median values of the Si/Al ratio do not differ substantially between the flights; however, the mean value displays a clear peak during B764. The spread in the Si/Al ratio increases almost monotonically for the first five cases, with the maximum range displayed in B765. The K/Al and Ca/Al ratios are

ACPD
15, 29403–29453, 2015

especially heightened in the B768 case, and show consistency across each other case with the exception of B762. A comparable trend is also evident with the Fe/Si ratio and the Mg/Si ratio is slightly raised for cases B764 and B765.

3.4 Comparison between below and above cloud samples

The samples detailed previously were all exposed below cloud and were chosen as the particles collected likely influenced the cloud microphysics of clouds that formed above these exposure altitudes. Most of these cases appear to be influenced by local sources; cases B764 and B765 in particular are predominantly composed of fresh chlorides. However, these cases do not obviously address the involvement of aerosol particles from distant sources.

As a test case, a filter pair exposed above cloud was analysed to compare the particle compositions. A case study was chosen: flight B764 provided consecutive filter exposures below and above a stratus cloud deck, approximately one hour apart, allowing a comparison between the respective compositional characteristics. The cloud located between the exposures was mixed-phase, with a sub-adiabatic CDP liquid-water content profile measured. This suggests that entrainment of aerosol from above may be an important source contributing to changes in the cloud microphysical properties in this case (Jackson et al., 2012), or that the liquid-water in the cloud has been depleted via precipitation processes. The air-mass back trajectories varied little between the exposures, with both cases influenced by air from over the Barents Sea and the coast of Northern Russia (see Fig. 3). The conditions sampled during each of these exposures are summarised in Table 5.

Figure 8 highlights the differences between the below and above cloud samples. The fraction of unclassified particles is greater in the above cloud example for sizes $> 0.5\,\mu m$ (panel b), whilst a similar fraction was observed in both cases for sizes $\leq 0.5\,\mu m$ (panel a). Similarly, a comparable fraction of silicates is found on both filter pairs. Greater fractions of fresh chlorides are found on the below cloud sample; however, a moderate loading of sea salt – and aged sea salt – is still identified in the

ACPD
15, 29403–29453, 2015

above cloud case. The above cloud exposure also has a greater sulphate loading and the absolute number of particles detected was lower than in the below cloud case. The size-segregated classifications shown in panel c of Fig. 8 display significant unclassified fractions across most sizes, with increased contributions at <1 and $>3\,\mu m$. The dominating species changes from unclassified to fresh chlorides to silicates as particle size increases and significant mixed chloride fractions were also observed at small sizes.

4 Discussion

4.1 Case overview

The filter-derived and probe-averaged size distributions from Sect. 3.2 compare reasonably well. The disagreement at the size limits (<0.5 and $>10\,\mu m$) of these distributions implies that collection issues (e.g. from the sub-isokinetic sampling) are influencing these samples. It is also probable that sub-micron particles either pass through the filter pores at the time of exposure or are left undetected by the EDS analysis due to a decreasing signal-to-noise ratio with decreasing particle size (Kandler et al., 2007). It is therefore concluded that the extremes of the particle size distribution collected by the filters and analysed by the ESEM/EDS system are under-represented. This is the same conclusion reached by Johnson et al. (2012) for their ESEM/EDS comparison with airborne particle measurements, whose samples were analysed using the same facilities in the Williamson Research Centre. Similarly, the size characteristics of the aerosol particles collected by Chou et al. (2008) compared reasonably well – within a 1-σ confidence level – with measurements from optical particle counters mounted externally on their measurement aircraft. Crucially, Chou et al. (2008) found that their accumulation-mode filter size distributions derived from Transmission Electron Microscopy (TEM) correlated better with observational data obtained from a cabin-based PCASP variation (CVI-PCASP) than their ESEM-derived distributions.

ACPD
15, 29403–29453, 2015

Given the similarity between the filtration techniques applied, this may suggest that the disagreement between the accumulation-mode distributions observed in this study could be a result of the limitations of the ESEM technique rather than an issue with the filter sampling from the aircraft. However, Chou et al. (2008) also identified differences between the performance of their CVI-PCASP and externally-mounted PCASP – with the former consistently over-counting compared to the latter – suggesting that possible inlet losses could be similarly affecting the wing-mounted PCASP used in this study. In summary, the ESEM technique, the filter mechanism collection efficiency and possible inlet losses could all be introducing some magnitude of error to the comparisons shown in Fig. 4, and it is not trivial to identify which source of error is the most influential in these cases.

4.1.1 Cases B760–B765

The compositional trends observed in Figs. 5 and 6 are typically different between each flight. Compositional dominance varies from sulphates to silicates to fresh chlorides through the first five cases. The difference between dominant classifications at sizes less than or greater than 0.5 µm is clear (Fig. 5), and Kandler et al. (2009) observed a similar size dependence in their sample. They also observed a distinct shift in average composition of particles at the 0.5 µm diameter limit, where the principal compositions in their African sample switched from sulphates to silicates and other minerals.

The influence of sulphates, silicates and fresh chlorides varies substantially in the first five flights; variability which could be inferred from the differences in the respective back trajectories. There are distinct similarities between the trends derived for the B764 and B765 cases, with dominant fresh chloride and silicate signatures observed (Fig. 6). Both cases also display a similar loading of mixed chlorides at sizes > 0.5 µm (Fig. 5); particles which are likely sea salts mixed with sulphates. The chloride classifications are not ubiquitously observed in the first five cases, with particularly low measurements of these species in B760 and B761. This suggests that the ocean was not a strong source of aerosol particles in these cases, whereas the significance of this source is

ACPD
15, 29403–29453, 2015

clear in cases B762, B764 and B765. This hypothesis is strengthened by the back trajectories calculated for these exposures (Fig. 3); the air-mass source for the B760 and B761 cases was the frozen Arctic Ocean, whilst cases B764 and B765 both had low-altitude trajectories across the sea surface. During the transition over the ocean, sea salts could have been lifted into the air stream. The B760 case displays a high sulphates signature at sub-micron sizes – a characteristic unique from the other cases – suggesting that the particles had sufficient time to interact with sulphate gases (from either anthropogenic or marine sources, see Sect. 2.4.2) during transit over the frozen Arctic Ocean. There is a common link between the first three cases in their respective silicate loadings; the measured amount of silicate-based dusts was high in these cases, with a maximum reached during B761.

4.1.2 Case B768

The B768 sample was collected in a slightly different location – to the north-west of Svalbard instead of the south-east – than the first five cases (see Table 1). The particle loading was much greater for this case, as illustrated clearly by the filter-derived size distributions shown in Fig. 4. Additionally, there are distinct compositional differences between the first five cases and the B768 case. This case is the only one not to be dominated by silicates at super-micron sizes and it was found to have the greatest proportion of Ca-rich particles, biomass tracers and unclassified particles across the sizes considered. The B768 case is unique in its dominant particle categories, their respective size evolution and air mass back trajectory, emphasising its contrast to the other cases. This is particularly clear with the sub-micron particles detected (Fig. 5).

The magnitude of the biomass tracer fraction was only sufficient enough to be observed in the B768 case. These particles are more prevalent at small sizes, as seen in Fig. 5. Andreae (1983) have previously shown that there is a strong relationship between biomass particle species and particle size below 2 µm. The K measurements in these particles mirror the quantities measured by Umo et al. (2015) for bottom ashes, adding confidence to their identification as biomass products. The modelled back tra-

ACPD
15, 29403–29453, 2015

jectory for the B768 case hailed from Northern Russia and the European continent. A potential source of these particles could be from similar boreal forest fire events to those sampled by Quennehen et al. (2012), which was also observed at approximately the same time of year, or from European biomass activities.

The Ca-rich particles observed strongly in B768 are distinct and not observed to the same magnitude in the other flights, implying a unique source. It is possible that these are naturally-occurring carbonate dusts; however, Umo et al. (2015) also measured several species of Ca-based dusts in their wood and bottom ash samples, suggesting that these could also be sourced from biomass burning activities. The strong detection of Ca-rich particles alongside the K-dominant biomass particles supports this conclusion in this case. The relative prevalence of K-rich and Ca-rich particles found in the sub- and super-micron ranges mirrors the relationship observed in the biomass burning study by Andreae (1983). The large Ca signature is also observed in the silicate and mixed silicate spectra for this case (Fig. S1 in the Supplement), and consequently affects the K/Al and Ca/Al ratios (shown in Fig. 7). It is unclear whether these enhanced values are a result of internal mixing of some silicates with the Ca- or K-rich biomass particles or if they are real feldspar signatures (as K-feldspar or plagioclase). The Fe/Si ratio is also elevated for this case and this could be due to increased detection of clay-like dusts or Hematite, and/or internal mixing with anthropogenic smelting emissions.

4.2 Sourcing the dust

Unexpectedly, large fractions of silicate dusts were observed – to different extents – in every case. These filters were collected in March when the majority of the surrounding surface was snow-covered, therefore there is no obvious local source of mineral dust. Weinbruch et al. (2012) also identified large dust fractions in their samples collected at Ny Ålesund in April 2008, and these dusts would likely act as a source of ice nucleating particles for clouds in this region. The presence of dust in such quantities could either be due to some local source, long-range transport or a combination of these two

ACPD
15, 29403–29453, 2015

avenues. To better understand the characteristics of these dusts, the elemental ratios in Fig. 7 can be considered. In general, the consistency in the median Si/Al ratio between each case suggests that the typical composition of the aluminosilicates has low variability, with each distribution skewed differently to account for the differences in the mean and variance values.

Elemental ratios can be used to infer a source of the mineral dusts, and several studies have investigated characteristic ratios of dusts from a variety of arid regions. For example, the African dust study by Formenti et al. (2008) calculated these ratios from airborne filter data and derived Si/Al, K/Al and Ca/Al ratios of approximately 3, 0.25 and 0.5 respectively. These values are within the limits of those calculated in this study (Fig. 7); however, a lack of good agreement suggests that these sources may not be related to the dusts analysed here. Zhang et al. (2001) presented these ratios for dusts collected at various Asian sites, and their Tibetan and Loess Plateau samples were found to have Si/Al ratios of 4.6 and 2.5 respectively. The Loess values are more consistent with the mean values obtained from B760, B761 and B768, whereas the Tibetan values lie within the upper bounds of samples B762, B764 and B765. The Loess samples also had a Ca/Al ratio of 2.7, which lies between the median and mean values obtained for B768, and is within the upper bound of B762; however, it is much greater than the average ratio derived for the majority of the cases presented. The K/Al ratio was found to be 0.95, consistent with the first five cases but not B768. This could be due to the heightened K influence in B768 from biomass sources, but could also be coincidental and care must be taken when attributing a transported dust sample to a given source via this method. The dust collected by the aircraft filters during ACCACIA does appear to have more in common with the Asian samples than the African samples; however, the composition of dusts originating from the same source region is not always consistent and can vary quite substantially between close geographical locations (Glen and Brooks, 2013). It is also unclear how these ratios would be affected by transportation, as atmospheric processing will likely alter the composition of ageing dust with respect to the freshly-emitted dust samples mentioned here.

ACPD
15, 29403–29453, 2015

Despite this, it is worth noting that Liu et al. (2015) identified high-altitude plumes during the springtime ACCACIA campaign which hailed from the Asian continent. It could be possible that dusts from these sources were advected over large distances in addition to the black carbon explicitly measured and modelled by Liu et al. (2015). The increase in mean trajectory altitude with time, as shown in Fig. 3, supports this theory as the descent of air from > 1000 m could be drawing dusts down to the low-altitudes considered. The theory that Asian dust contributes to the Arctic Haze is not new, and some observations indicate that this is the case (e.g. Rahn et al., 1977), yet models have not been able to produce conclusive evidence (Quinn et al., 2007). A key question in this hypothesis is theorising how the dust travels up to high altitudes in the atmosphere, and subsequently undergoes this long-range transportation, without experiencing cloud processing. It is possible that frontal uplifts at the source are responsible, with weakly-scavenging mixed-phase clouds along the trajectories allowing the dust loading to remain so high.

4.3 Internally-mixed aerosol particles

The degree of internal mixing in each case is different – as displayed by the variability in mean fractions shown in Fig. S1 in the Supplement – thus tying in with the differences between the air mass histories. Particles which have undergone long-range transport likely have enhanced internal mixing, and may not be adequately classified by the scheme employed in this study. Unclassified particles are prevalent in the B761, B762 and B768 below-cloud cases (Figs. 5 and 6). The variability within the categories (as seen in Fig. S1 in the Supplement) highlights the importance of treating the classifications with caution: they provide a good representation of the particle species collected, yet the ability of the classification criteria to accurately account for internally-mixed species is not always efficient. The extent of the unclassified category must always be considered to account for this.

The influence of internally-mixed, transported particles on the population is most evident from the higher-altitude case: the B764 above-cloud sample detailed in Fig. 8 is

ACPD
15, 29403–29453, 2015

distinctly different from its below-cloud counterpart (Fig. 6). In addition to the enhanced other fraction, large mixed chloride, sulphate and mixed silicate loadings were also identified (Fig. 8); classifications which could be attributed to anthropogenic influences. The contrast between the below and above cloud cases emphasises the segregation of the Arctic aerosol sources: whilst being influenced by local surface sources, the Arctic atmosphere is also affected by this influx of long-range transported aerosol particles – the Arctic Haze – during the spring months (Barrie, 1986; Shaw, 1995; Liu et al., 2015). Both of these aerosol pathways will affect the cloud microphysics, and further investigation is required to better understand the importance of each.

The differences in composition between the below and above cloud samples can be explained by the presence of the cloud in between: the particles present would have interacted with the cloud as CCN or INPs, and so the cloud inhibited the direct mixing of these two aerosol populations. This could have unclear consequences for the resultant cloud microphysics as internally-mixed particles (e.g. with some mineral constituent) could act as INPs or (Giant) CCN dependent on the mixing state and the hygroscopicity of the particle (see Sect. 2.4.3). A complex particle is difficult to clearly categorise as an INP or CCN as its nucleation will be heavily dependent on the environmental conditions. The presence of coatings on particles can also have a significant impact on their role in aerosol-cloud interactions. Coatings of soluble material could enhance CCN ability and promote secondary ice production via the formation of large cloud drops (Levin et al., 1996), whilst organic coatings could suppress the nucleating ability of an efficient INP (Möhler et al., 2008).

The complexity of internal and external mixing observed indicates that some INP predictions may be fraught with inaccuracy in this region; for example, DeMott et al. (2010) relate INP concentration to the total aerosol concentration $> 0.5\,\mu m$ under the assumption that most of the particles in this limit are INPs. However, efficient INPs (e.g. mineral dusts) were not found to be consistently dominant in this study. As suggested by DeMott et al. (2010), this relation may not be applicable in cases heavily influenced by marine sources, and the high loadings of super-micron sea salt identified in some

ACPD
15, 29403–29453, 2015

of the ACCACIA cases would qualify these as such. The use of dust-based parameterisations such as Niemand et al. (2012) or DeMott et al. (2015) may provide a more accurate prediction of the INP concentration in these cases. Despite this, the ice nucleating ability of the unclassified and mixed particle categories is not quantifiable in this study and it is likely that they would influence the INP population; whilst soluble coatings may suppress ice nucleating ability, the presence of IN-active coatings and/or complex internal-mixing could act to enhance it. Examples of IN-active coatings could include biological material, as some strains of bacteria have been observed to be efficient INPs in laboratory studies (Möhler et al., 2007; Hoose and Möhler, 2012). Some studies have identified cases where bacteria has survived long-range atmospheric transport by piggybacking dust particles (Yamaguchi et al., 2012). It is possible that such bacteria could influence the Arctic atmosphere via a similar transportation mechanism. Fundamentally, comprehending how these internally-mixed particles interact and impact the cloud microphysics is a significant step to take towards improving our understanding of aerosol-cloud interactions in the Arctic springtime.

5 Conclusions

During the Aerosol-Cloud Coupling and Climate Interactions (ACCACIA) springtime campaign, in-situ samples of Arctic aerosol particles were collected on polycarbonate filters. Analysis of these samples has been detailed, with a focus placed upon identifying the composition of the collected particles and investigating their potential sources. In total, six below-cloud exposures were analysed to infer how the local sources may influence the cloud microphysics of the region (Fig. 1). Additionally, one above-cloud filter pair was analysed to investigate the composition of transported particles (Fig. 8). The main findings of this study are as follows:

– Single-particle analysis of the filters produced number size distributions which were comparable to those derived from the wing-mounted optical particle coun-

ACPD
15, 29403–29453, 2015

ters (Fig. 4). The composition of the particles collected was strongly dependent upon size across all samples, with crustal minerals and sea salts dominating the super-micron range. Carbon- and sulphur-based particles were prevalent in the $< 0.5\,\mu m$ limit (Fig. 5). Large fractions of complex internal mixtures – as shown by the other, mixed silicate and mixed chloride categories in Figs. 5 and 6 – were identified in each case as expected. The impact of these particles on cloud microphysics as potential INPs and/or CCN is not quantifiable by this study; however, it is likely that the silicate dusts identified would act as a source of INPs for clouds in this region.

– There are distinct size-dependent compositional trends observed in each sample, with stark differences between cases (Fig. 6). These differences were attributed to variations in the air mass histories; cases B760 and B761 presented a clear silicate dust dominance and the B764 and B765 cases were found to have very similar chloride and silicate abundances. These similarities were mirrored by their closely-related source regions (Fig. 3). The relationship between composition and trajectory was strengthened by the unique attributes of the B768 case; both the trends and trajectory were distinct in this case, and the particle classifications identified can be explained by hypothesised sources along the trajectory presented.

– Crustal minerals were identified in all cases, despite the seasonal local snow cover. The HYSPLIT back trajectories (Fig. 3) were variable in direction, yet typically increased in mean altitude over time. Therefore, these dusts were hypothesised to have undergone long-range, high-altitude transport from distant sources, through regions containing weakly-scavenging mixed-phase clouds. Some elemental characteristics (Fig. 7) were found to be consistent with Asian dust sources; however, it is not known how long-range transport may affect the composition of these dusts and so this theory cannot be proven with this data.

ACPD
15, 29403–29453, 2015

The coarse-mode, non-volatile Arctic aerosol particles analysed by this study showed great variation between subsequent days and different meteorological conditions, therefore it would be difficult to incorporate these findings into models. However, the measurements from the springtime ACCACIA campaign provide a good opportunity to simultaneously investigate both the properties of aerosol particles in the region and the microphysical characteristics of the clouds observed. Further study of the cloud microphysics of these cases, with reference to these aerosol observations, will allow us to improve the representation of aerosol-cloud interactions in climate models and act to reduce the uncertainty in forecasting the Arctic atmosphere in the future.

The Supplement related to this article is available online at doi:10.5194/acpd-15-29403-2015-supplement.

Acknowledgements. This work was funded by the National Environment Research Council (NERC), under grant NE/I028696/1, as part of the ACCACIA campaign. G. Young was supported by a NERC PhD studentship. We would like to thank the ACCACIA project team for their efforts. Airborne data were obtained using the BAe-146-301 Atmospheric Research Aircraft [ARA] flown by Directflight Ltd and managed by the Facility for Airborne Atmospheric Measurements [FAAM], which is a joint entity of the Natural Environment Research Council [NERC] and the Met Office. G. Young would also like to thank J. Fellowes and J. Waters at the Williamson Research Centre for their guidance with the ESEM instrument and the European Geosciences Union for funding the publication this article as part of an OSP 2015 award.

References

Andreae, M. O.: Soot Carbon and Excess Fine Potassium: Long-Range Transport of Combustion-Derived Aerosols, Science, 220, 1148–1151, doi:10.1126/science.220.4602.1148, 1983. 29417, 29418, 29425, 29426

ACPD
15, 29403–29453, 2015

Andreae, M. O. and Rosenfeld, D.: Aerosol cloud precipitation interactions. Part 1. The nature and sources of cloud-active aerosols, Earth Sci. Rev., 89, 13–41, doi:10.1016/j.earscirev.2008.03.001, 2008. 29406, 29415

Andreae, M. O., Elbert, W., Gabriel, R., Johnson, D. W., Osborne, S., and Wood, R.: Soluble ion chemistry of the atmospheric aerosol and SO concentrations over the eastern North Atlantic during ACE-2, Tellus B, 52, 1066–1087, doi:10.1034/j.1600-0889.2000.00105.x, 2000. 29409

Barrie, L. A.: Arctic Air Chemistry: An Overview, in: Arctic Air Pollution, edited by: Stonehouse, B., Cambridge University Press, Cambridge, UK, 1986. 29406, 29429

Behrenfeldt, U., Krejci, R., Ström, J., and Stohl, A.: Chemical properties of Arctic aerosol particles collected at the Zeppelin station during the aerosol transition period in May and June of 2004, Tellus B, 60, 405–415, doi:10.1111/j.1600-0889.2008.00349.x, 2008. 29406, 29411, 29412, 29413, 29414, 29416

Chou, C., Formenti, P., Maille, M., Ausset, P., Helas, G., Harrison, M., and Osborne, S.: Size distribution, shape, and composition of mineral dust aerosols collected during the African Monsoon Multidisciplinary Analysis Special Observation Period 0: Dust and Biomass-Burning Experiment field campaign in Niger, January 2006, J. Geophys. Res., 113, D00C10, doi:10.1029/2008JD009897, 2008. 29409, 29410, 29417, 29419, 29423, 29424

Connolly, P. J., Möhler, O., Field, P. R., Saathoff, H., Burgess, R., Choularton, T., and Gallagher, M.: Studies of heterogeneous freezing by three different desert dust samples, Atmos. Chem. Phys., 9, 2805–2824, doi:10.5194/acp-9-2805-2009, 2009. 29405

Conny, J. M. and Norris, G. A.: Scanning Electron Microanalysis and Analytical Challenges of Mapping Elements in Urban Atmospheric Particles, Environ. Sci. Technol., 45, 7380–7386, doi:10.1021/es2009049, 2011. 29415

Crosier, J., Allan, J. D., Coe, H., Bower, K. N., Formenti, P., and Williams, P. I.: Chemical composition of summertime aerosol in the Po Valley (Italy), northern Adriatic and Black Sea, Q. J. Roy. Meteor. Soc., 133, 61–75, doi:10.1002/qj.88, 2007. 29410

Curry, J. A., Rossow, W. B., Randall, D., and Schramm, J. L.: Overview of Arctic Cloud and Radiation Characteristics., J. Climate, 9, 1731–1764, doi:10.1175/1520-0442(1996)009<1731:OOACAR>2.0.CO;2, 1996. 29404, 29405

de Boer, G., Shupe, M. D., Caldwell, P. M., Bauer, S. E., Persson, O., Boyle, J. S., Kelley, M., Klein, S. A., and Tjernström, M.: Near-surface meteorology during the Arctic Summer Cloud

ACPD
15, 29403–29453, 2015

Ocean Study (ASCOS): evaluation of reanalyses and global climate models, Atmos. Chem. Phys., 14, 427–445, doi:10.5194/acp-14-427-2014, 2014. 29405
DeMott, P. J., Prenni, A. J., Liu, X., Kreidenweis, S. M., Petters, M. D., Twohy, C. H., Richardson, M. S., Eidhammer, T., and Rogers, D. C.: Predicting global atmospheric ice nuclei distributions and their impacts on climate, P. Natl. Acad. Sci. USA, 107, 11217–11222, doi:10.1073/pnas.0910818107, 2010. 29405, 29429
DeMott, P. J., Prenni, A. J., McMeeking, G. R., Sullivan, R. C., Petters, M. D., Tobo, Y., Niemand, M., Möhler, O., Snider, J. R., Wang, Z., and Kreidenweis, S. M.: Integrating laboratory and field data to quantify the immersion freezing ice nucleation activity of mineral dust particles, Atmos. Chem. Phys., 15, 393–409, doi:10.5194/acp-15-393-2015, 2015. 29430
Draxler, R. R. and Hess, G. D.: An Overview of the HYSPLIT_4 Modelling System for Trajectories, Dispersion, and Deposition, Aust. Meteorol. Mag., 47, 295–308, 1998. 29409
Fleming, Z. L., Monks, P. S., and Manning, A. J.: Review: Untangling the influence of airmass history in interpreting observed atmospheric composition, Atmos. Res., 104, 1–39, doi:10.1016/j.atmosres.2011.09.009, 2012. 29409
Formenti, P., Rajot, J. L., Desboeufs, K., Caquineau, S., Chevaillier, S., Nava, S., Gaudichet, A., Journet, E., Triquet, S., Alfaro, S., Chiari, M., Haywood, J., Coe, H., and Highwood, E.: Regional variability of the composition of mineral dust from western Africa: Results from the AMMA SOP0/DABEX and DODO field campaigns, J. Geophys. Res., 113, D00C13, doi:10.1029/2008JD009903, 2008. 29409, 29427
Formenti, P., Schütz, L., Balkanski, Y., Desboeufs, K., Ebert, M., Kandler, K., Petzold, A., Scheuvens, D., Weinbruch, S., and Zhang, D.: Recent progress in understanding physical and chemical properties of African and Asian mineral dust, Atmos. Chem. Phys., 11, 8231–8256, doi:10.5194/acp-11-8231-2011, 2011. 29411, 29416
Geng, H., Ryu, J., Jung, H.-J., Chung, H., Ahn, K.-H., and Ro, C.-U.: Single-Particle Characterization of Summertime Arctic Aerosols Collected at Ny-Ålesund, Svalbard, Environ. Sci. Technol., 44, 2348–2353, doi:10.1021/es903268j, 2010. 29406, 29413, 29414
Glen, A. and Brooks, S. D.: A new method for measuring optical scattering properties of atmospherically relevant dusts using the Cloud and Aerosol Spectrometer with Polarization (CASPOL), Atmos. Chem. Phys., 13, 1345–1356, doi:10.5194/acp-13-1345-2013, 2013. 29408, 29427
Hand, V. L., Capes, G., Vaughan, D. J., Formenti, P., Haywood, J. M., and Coe, H.: Evidence of internal mixing of African dust and biomass burning particles by individ-

ACPD
15, 29403–29453, 2015

ual particle analysis using electron beam techniques, J. Geophys. Res., 115, D13301, doi:10.1029/2009JD012938, 2010. 29410, 29411, 29412, 29413, 29414, 29416, 29417

Heintzenberg, J., Hansson, H.-C., Ogren, J. A., Covert, D. S., Blanchet, J.-P.: Physical and Chemical Properties of Arctic Aerosols and Clouds, in: Arctic Air Pollution, edited by: Stonehouse, B., Cambridge University Press, Cambridge, UK, 1986. 29405

Hoose, C. and Möhler, O.: Heterogeneous ice nucleation on atmospheric aerosols: a review of results from laboratory experiments, Atmos. Chem. Phys., 12, 9817–9854, doi:10.5194/acp-12-9817-2012, 2012. 29405, 29415, 29430

IPCC AR5: Clouds and Aerosols, in: Climate Change 2013: The Physical Science Basis, Contribution of Working Group I to the Fifth Assessment Report of the Intergovernmental Panel on Climate Change, edited by: Boucher, O., Randall, D., Artaxo, P., Bretherton, C., Feingold, G., Forser, P., Kerminen, V. M., Kondo, Y., Liao, H., Lohmann, U., Rasch, P., Satheesh, S. K., Sherwood, S., Stevens, B., Zhang, X. Y., and (Stocker, T. F., Qin, D., Plattner, G. K., Tignor, M., Allen,S. K., Boschung, J., Nauels, A., Xia, Y., Bex, V., and Midley, P. M., Cambridge University Press, Cambridge, United Kingdom and New York, NY, USA, doi:10.1017/CBO9781107415324.016, 2013. 29405

Jackson, R. C., McFarquhar, G. M., Korolev, A. V., Earle, M. E., Liu, P. S. K., Lawson, R. P., Brooks, S., Wolde, M., Laskin, A., and Freer, M.: The dependence of ice microphysics on aerosol concentration in arctic mixed-phase stratus clouds during ISDAC and M-PACE, J. Geophys. Res., 117, D15207, doi:10.1029/2012JD017668, 2012. 29422

John, W., Hering, S., Reischl, G., Sasaki, G., and Goren, S.: Characteristics of Nuclepore filters with large pore size – II. Filtration properties, Atmos. Environ., 17, 373–382, doi:10.1016/0004-6981(83)90054-9, 1983. 29410

Johnson, B., Turnbull, K., Brown, P., Burgess, R., Dorsey, J., Baran, A. J., Webster, H., Haywood, J., Cotton, R., Ulanowski, Z., Hesse, E., Woolley, A., and Rosenberg, P.: In situ observations of volcanic ash clouds from the FAAM aircraft during the eruption of Eyjafjallajökull in 2010, J. Geophys. Res., 117, D00U24, doi:10.1029/2011JD016760, 2012. 29409, 29410, 29423

Kandler, K., Benker, N., Bundke, U., Cuevas, E., Ebert, M., Knippertz, P., Rodríguez, S., Schütz, L., and Weinbruch, S.: Chemical composition and complex refractive index of Saharan Mineral Dust at Izaña, Tenerife (Spain) derived by electron microscopy, Atmos. Environ., 41, 8058–8074, doi:10.1016/j.atmosenv.2007.06.047, 2007. 29411, 29412, 29413, 29416, 29420, 29423

ACPD
15, 29403–29453, 2015

Kandler, K., Schütz, L., Deutscher, C., Ebert, M., Hofmann, H., Jäckel, S., Jaenicke, R., Knippertz, P., Lieke, K., Massling, A., Petzold, A., Schladitz, A., Weinzierl, B., Wiedensohler, A., Zorn, S., and Weinbruch, S.: Size distribution, mass concentration, chemical and mineralogical composition and derived optical parameters of the boundary layer aerosol at Tinfou, Morocco, during SAMUM 2006, Tellus B, 61, 32–50, doi:10.1111/j.1600-0889.2008.00385.x, 2009. 29424

Kandler, K., Lieke, K., Benker, N., Emmel, C., Küpper, M., Müller-Ebert, D., Ebert, M., Scheuvens, D., Schladitz, A., Schütz, L., and Weinbruch, S.: Electron microscopy of particles collected at Praia, Cape Verde, during the Saharan Mineral Dust Experiment: particle chemistry, shape, mixing state and complex refractive index, Tellus B, 63, 475–496, doi:10.1111/j.1600-0889.2011.00550.x, 2011. 29412, 29413, 29421

Kanji, Z. A., Welti, A., Chou, C., Stetzer, O., and Lohmann, U.: Laboratory studies of immersion and deposition mode ice nucleation of ozone aged mineral dust particles, Atmos. Chem. Phys., 13, 9097–9118, doi:10.5194/acp-13-9097-2013, 2013. 29405

Krejci, R., Ström, J., de Reus, M., and Sahle, W.: Single particle analysis of the accumulation mode aerosol over the northeast Amazonian tropical rain forest, Surinam, South America, Atmos. Chem. Phys., 5, 3331–3344, doi:10.5194/acp-5-3331-2005, 2005. 29412, 29413

Krueger, B. J., Grassian, V. H., Laskin, A., and Cowin, J. P.: The transformation of solid atmospheric particles into liquid droplets through heterogeneous chemistry: Laboratory insights into the processing of calcium containing mineral dust aerosol in the troposphere, Geophys. Res. Lett., 30, 1148, doi:10.1029/2002GL016563, 2003. 29415

Lance, S., Brock, C. A., Rogers, D., and Gordon, J. A.: Water droplet calibration of the Cloud Droplet Probe (CDP) and in-flight performance in liquid, ice and mixed-phase clouds during ARCPAC, Atmos. Meas. Tech., 3, 1683–1706, doi:10.5194/amt-3-1683-2010, 2010. 29408

Levin, Z., Ganor, E., and Gladstein, V.: The Effects of Desert Particles Coated with Sulfate on Rain Formation in the Eastern Mediterranean., J. Appl. Meteorol., 35, 1511–1523, doi:10.1175/1520-0450(1996)035<1511:TEODPC>2.0.CO;2, 1996. 29429

Levin, Z., Teller, A., Ganor, E., and Yin, Y.: On the interactions of mineral dust, sea-salt particles, and clouds: A measurement and modeling study from the Mediterranean Israeli Dust Experiment campaign, J. Geophys. Res., 110, D20202, doi:10.1029/2005JD005810, 2005. 29416

ACPD
15, 29403–29453, 2015

Li, J., Pósfai, M., Hobbs, P. V., and Buseck, P. R.: Individual aerosol particles from biomass burning in southern Africa: 2, Compositions and aging of inorganic particles, J. Geophys. Res., 108, 8484, doi:10.1029/2002JD002310, 2003. 29412

Liu, B. Y. H. and Lee, K. W.: Efficiency of membrane and nuclepore filters for submicrometer aerosols, Environ. Sci. Technol., 10, 345–350, doi:10.1021/es60115a002, 1976. 29410

Liu, D., Quennehen, B., Darbyshire, E., Allan, J. D., Williams, P. I., Taylor, J. W., Bauguitte, S. J.-B., Flynn, M. J., Lowe, D., Gallagher, M. W., Bower, K. N., Choularton, T. W., and Coe, H.: The importance of Asia as a source of black carbon to the European Arctic during springtime 2013, Atmos. Chem. Phys., 15, 11537–11555, doi:10.5194/acp-15-11537-2015, 2015. 29406, 29408, 29409, 29428, 29429

Lloyd, G., Choularton, T. W., Bower, K. N., Crosier, J., Jones, H., Dorsey, J. R., Gallagher, M. W., Connolly, P., Kirchgaessner, A. C. R., and Lachlan-Cope, T.: Observations and comparisons of cloud microphysical properties in spring and summertime Arctic stratocumulus clouds during the ACCACIA campaign, Atmos. Chem. Phys., 15, 3719–3737, doi:10.5194/acp-15-3719-2015, 2015. 29408

Mamane, Y. and Noll, K. E.: Characterization of large particles at a rural site in the eastern United States: Mass distribution and individual particle analysis, Atmos. Environ., 19, 611–622, doi:10.1016/0004-6981(85)90040-X, 1985. 29413, 29416, 29420

Möhler, O., DeMott, P. J., Vali, G., and Levin, Z.: Microbiology and atmospheric processes: the role of biological particles in cloud physics, Biogeosciences, 4, 1059–1071, doi:10.5194/bg-4-1059-2007, 2007. 29430

Möhler, O., Benz, S., Saathoff, H., Schnaiter, M., Wagner, R., Schneider, J., Walter, S., Ebert, V., and Wagner, S.: The effect of organic coating on the heterogeneous ice nucleation efficiency of mineral dust aerosols, Environ. Res. Lett., 3, 025007, doi:10.1088/1748-9326/3/2/025007, 2008. 29429

Murray, B. J., O'Sullivan, D., Atkinson, J. D., and Webb, M. E.: Ice nucleation by particles immersed in supercooled cloud droplets., Chem. Soc. Rev., 41, 6519–6554, doi:10.1039/c2cs35200a, 2012. 29405, 29415

Niemand, M., Möhler, O., Vogel, B., Vogel, H., Hoose, C., Connolly, P., Klein, H., Bingemer, H., DeMott, P., Skrotzki, J., and Leisner, T.: A Particle-Surface-Area-Based Parameterization of Immersion Freezing on Desert Dust Particles, J. Atmos. Sci., 69, 3077–3092, doi:10.1175/JAS-D-11-0249.1, 2012. 29430

ACPD
15, 29403–29453, 2015

Perovich, D. K., Richter-Menge, J. A., Jones, K. F., and Light, B.: Sunlight, water, and ice: Extreme Arctic sea ice melt during the summer of 2007, Geophys. Res. Lett., 35, L11501, doi:10.1029/2008GL034007, 2008. 29404

Pruppacher, H. R. and Klett, J. D.: Microphysics of Clouds and Precipitation, 2nd ed., Kluwer Academic Publishers, Dordrecht, the Netherlands, 1997. 29405, 29407

Quennehen, B., Schwarzenboeck, A., Matsuki, A., Burkhart, J. F., Stohl, A., Ancellet, G., and Law, K. S.: Anthropogenic and forest fire pollution aerosol transported to the Arctic: observations from the POLARCAT-France spring campaign, Atmos. Chem. Phys., 12, 6437–6454, doi:10.5194/acp-12-6437-2012, 2012. 29417, 29426

Quinn, P. K., Shaw, G., Andrews, E., Dutton, E. G., Ruoho-Airola, T., and Gong, S. L.: Arctic haze: current trends and knowledge gaps, Tellus B, 59, 99–114, doi:10.1111/j.1600-0889.2006.00238.x, 2007. 29405, 29414, 29415, 29428

Rahn, K. A.: Relative importances of North America and Eurasia as sources of arctic aerosol, Atmos. Environ., 15, 1447–1455, doi:10.1016/0004-6981(81)90351-6, 1981. 29406

Rahn, K. A., Borys, R. D., and Shaw, G. E.: The Asian source of Arctic haze bands, Nature, 268, 713–715, doi:10.1038/268713a0, 1977. 29428

Reimann, C., Banks, D., and Caritat, P. D.: Impacts of Airborne Contamination on Regional Soil and Water Quality: The Kola Peninsula, Russia, Environ. Sci. Technol., 34, 2727–2732, doi:10.1021/es9912933, 2000. 29416

Rosenberg, P. D., Dean, A. R., Williams, P. I., Dorsey, J. R., Minikin, A., Pickering, M. A., and Petzold, A.: Particle sizing calibration with refractive index correction for light scattering optical particle counters and impacts upon PCASP and CDP data collected during the Fennec campaign, Atmos. Meas. Tech., 5, 1147–1163, doi:10.5194/amt-5-1147-2012, 2012. 29408

Seiler, W. and Crutzen, P.: Estimates of gross and net fluxes of carbon between the biosphere and the atmosphere from biomass burning, Climatic Change, 2, 207–247, doi:10.1007/BF00137988, 1980. 29418

Serreze, M. C., Holland, M. M., and Stroeve, J.: Perspectives on the Arctic's Shrinking Sea-Ice Cover, Science, 315, 1533–1536, doi:10.1126/science.1139426, 2007. 29404

Shaw, G. E.: The Arctic Haze Phenomenon., B. Am. Meteorol. Soc., 76, 2403–2414, doi:10.1175/1520-0477(1995)076<2403:TAHP>2.0.CO;2, 1995. 29406, 29429

Steinnes, E., Lukina, N., Nikonov, V., Aamlid, D., and Røyset, O.: A Gradient Study of 34 Elements in the Vicinity of a Copper-Nickel Smelter in the Kola Peninsula, Environ. Monit. Assess., 60, 71–88, doi:10.1023/A:1006165031985, 2000. 29414, 29417

ACPD
15, 29403–29453, 2015

Ström, J., Umegård, J., Tørseth, K., Tunved, P., Hansson, H.-C., Holmén, K., Wismann, V., Herber, A., and König-Langlo, G.: One year of particle size distribution and aerosol chemical composition measurements at the Zeppelin Station, Svalbard, March 2000–March 2001, Phys. Chem. Earth, 28, 1181–1190, doi:10.1016/j.pce.2003.08.058, 2003. 29406

Trembath, J. A.: Airborne CCN Measurements, PhD thesis, University of Manchester, Manchester, 2013. 29420

Umo, N. S., Murray, B. J., Baeza-Romero, M. T., Jones, J. M., Lea-Langton, A. R., Malkin, T. L., O'Sullivan, D., Neve, L., Plane, J. M. C., and Williams, A.: Ice nucleation by combustion ash particles at conditions relevant to mixed-phase clouds, Atmos. Chem. Phys., 15, 5195–5210, doi:10.5194/acp-15-5195-2015, 2015. 29417, 29425, 29426

Verlinde, J. Y., Harrington, J. Y., McFarquhar, G. M., Yannuzzi, V. T., Avramov, A., Greenberg, S., Johnson, N., Zhang, G., Poellot, M. R., Mather, J. H., Turner, D. D., Eloranta, E. W., Zak, B. D., Prenni, A. J., Daniel, J. S., Kok, G. L., Tobin, D. C., Holz, R., Sassen, K., Spangenberg, D., Minnis, P., Tooman, T. P., Ivey, M. D., Richardson, S. J., Bahrmann, C. P., Shupe, M., Demott, P. J., Heymsfield, A. J., and Schofield, R.: The Mixed-Phase Arctic Cloud Experiment, B. Am. Meteorol. Soc., 88, 205–221, doi:10.1175/BAMS-88-2-205, 2007. 29405

Vihma, T., Pirazzini, R., Fer, I., Renfrew, I. A., Sedlar, J., Tjernström, M., Lüpkes, C., Nygård, T., Notz, D., Weiss, J., Marsan, D., Cheng, B., Birnbaum, G., Gerland, S., Chechin, D., and Gascard, J. C.: Advances in understanding and parameterization of small-scale physical processes in the marine Arctic climate system: a review, Atmos. Chem. Phys., 14, 9403–9450, doi:10.5194/acp-14-9403-2014, 2014. 29406

Weinbruch, S., Wiesemann, D., Ebert, M., Schütze, K., Kallenborn, R., and Ström, J.: Chemical composition and sources of aerosol particles at Zeppelin Mountain (Ny Ålesund, Svalbard): An electron microscopy study, Atmos. Environ., 49, 142–150, doi:10.1016/j.atmosenv.2011.12.008, 2012. 29406, 29411, 29417, 29426

Yakobi-Hancock, J. D., Ladino, L. A., and Abbatt, J. P. D.: Feldspar minerals as efficient deposition ice nuclei, Atmos. Chem. Phys., 13, 11175–11185, doi:10.5194/acp-13-11175-2013, 2013. 29405, 29415

Yamaguchi, N., Ichijo, T., Sakotani, A., Baba, T., and Nasu, M.: Global Dispersion of Bacterial Cells on Asian Dust, Scientific Reports, 2, 525, doi:10.1038/srep00525, 2012. 29430

Zhang, X. Y., Arimoto, R., Cao, J. J., An, Z. S., and Wang, D.: Atmospheric dust aerosol over the Tibetan Plateau, J. Geophys. Res., 106, 18471, doi:10.1029/2000JD900672, 2001. 29427

ACPD
15, 29403–29453, 2015

Zhao, C., Klein, S. A., Xie, S., Liu, X., Boyle, J. S., and Zhang, Y.: Aerosol first indirect effects on non-precipitating low-level liquid cloud properties as simulated by CAM5 at ARM sites, Geophys. Res. Lett., 39, L08806, doi:10.1029/2012GL051213, 2012. 29405

Zimmermann, F., Weinbruch, S., Schütz, L., Hofmann, H., Ebert, M., Kandler, K., and Worringen, A.: Ice nucleation properties of the most abundant mineral dust phases, J. Geophys. Res., 113, D23204, doi:10.1029/2008JD010655, 2008. 29405, 29415

ACPD
15, 29403–29453, 2015

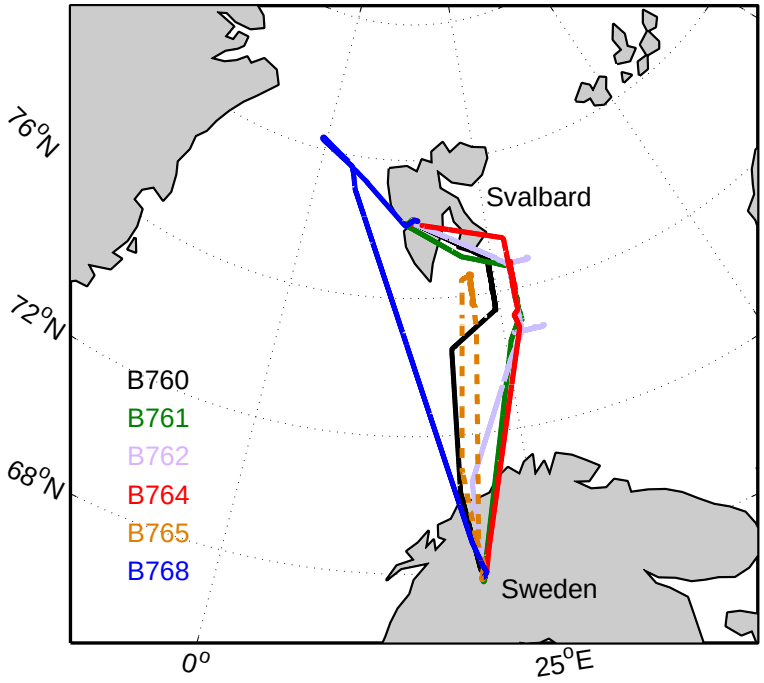

Figure 1. ACCACIA flight tracks of the main science periods undertaken for each flight where aerosol composition analysis was conducted.

ACPD
15, 29403–29453, 2015

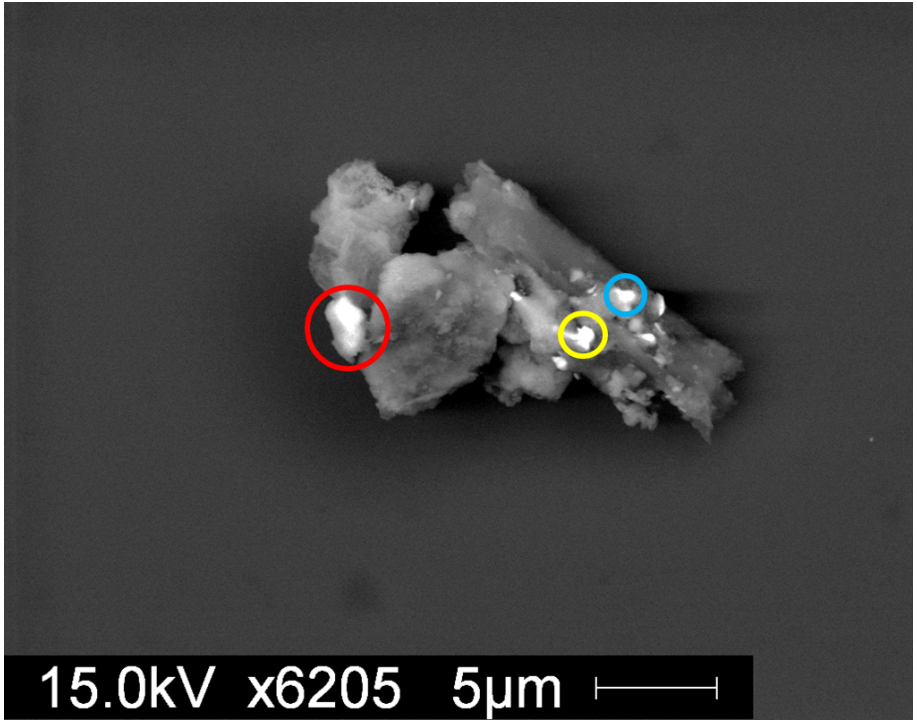

Figure 2. Well-mixed particle from B765. The circles denote the spots scanned to give the following dominating elements: Red – Fe, Si and Al; Yellow – Fe, Cr, Ni, Si and Al; Blue – Fe, Cr, Ca, Cl, S, Si and Al. Scan of full particle indicates Si dominance.

ACPD
15, 29403–29453, 2015

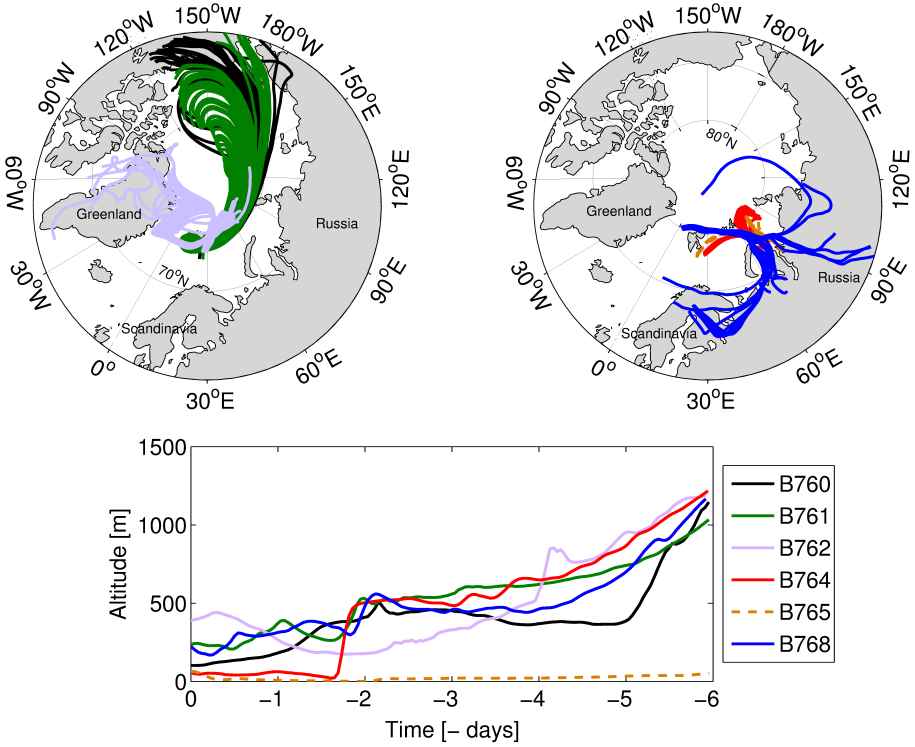

Figure 3. HYSPLIT air mass back trajectories for each of the 6 exposures, initialised at the aircraft's position and calculated 6 days backwards. Top left panel: B760 (black), B761 (green) and B762 (purple); top right panel: B764 (red), B765 (orange) and B768 (blue). The mean altitude covered by each of these trajectory groups is shown in the bottom panel.

ACPD
15, 29403–29453, 2015

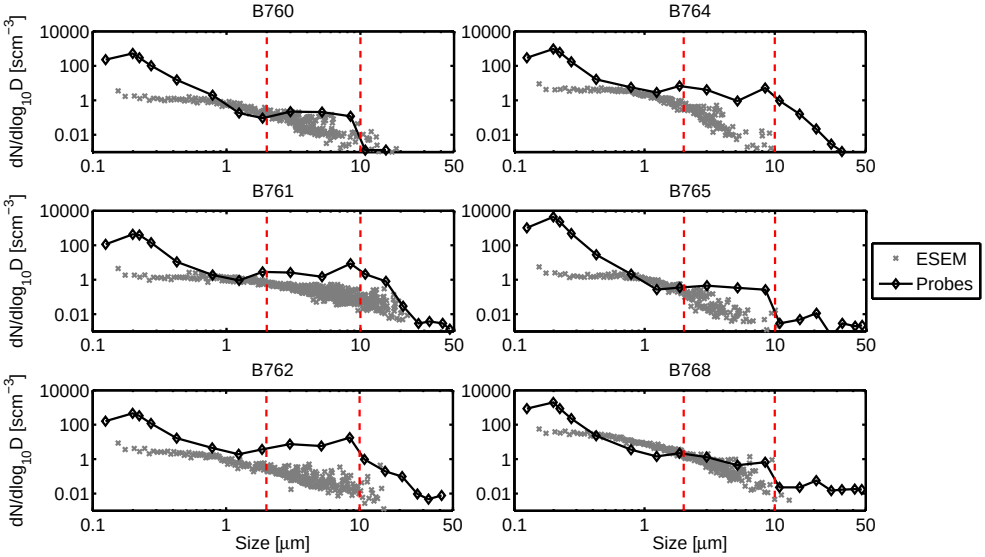

Figure 4. Size distributions ($dN/dlog_{10}D$) of particle data obtained via ESEM analysis compared with the averaged distributions derived from the optical particle counters at the relevant filter exposure times. Red lines mark the 2 and 10 µm thresholds where the probe data changes from PCASP to CAS-DPOL and from CAS-DPOL to CDP respectively. Probe data from cases B761, B762 and B764 show greater loadings at larger sizes due to some in-cloud sampling during the exposures; this heightens the likelihood that swollen aerosol particles and cloud droplets are measured by the externally-mounted CAS-DPOL and CDP.

ACPD
15, 29403–29453, 2015

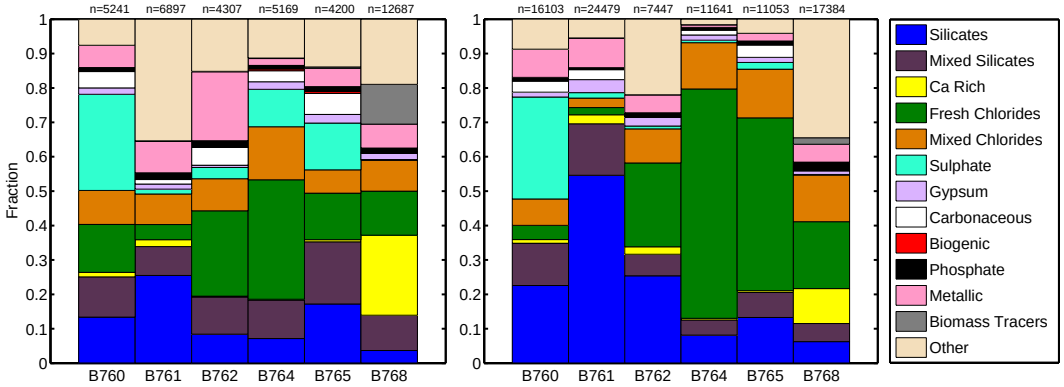

Figure 5. Averaged particle classifications from each sample. Each case is normalised to show the fraction (by number) that each given particle class occupies. The number of particles analysed are listed for each bin. Left panel: average $\leq 0.5\,\mu m$; right panel: average $> 0.5\,\mu m$.

ACPD
15, 29403–29453, 2015

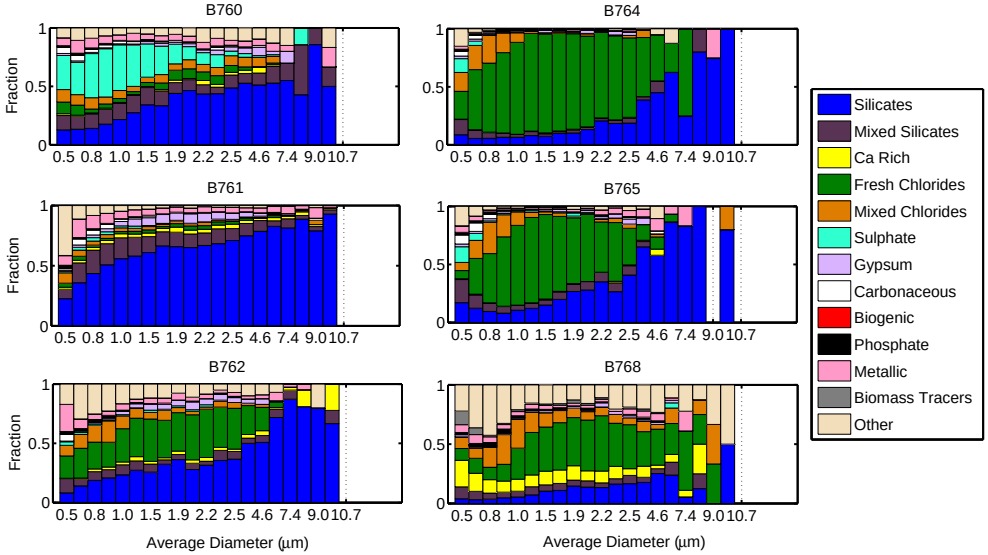

Figure 6. Size-segregated particle classifications applied to each below-cloud filter pair analysed from the considered flights, with each bin normalised to show the fraction (by number) occupied by each classification. The sizes indicated are the bin centres.

ACPD
15, 29403–29453, 2015

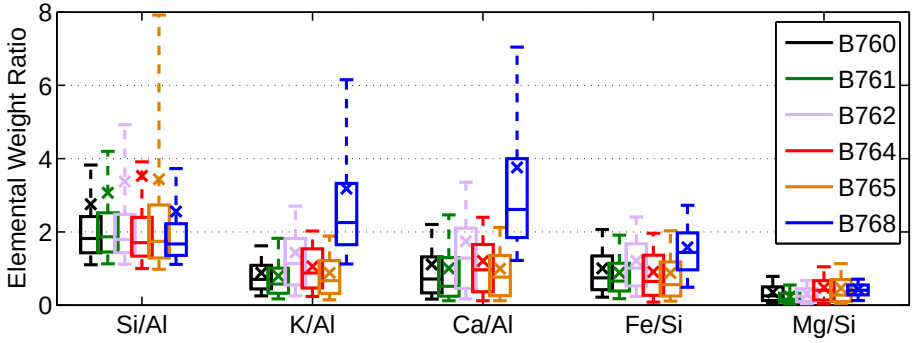

Figure 7. Mean elemental ratios from each flight. Only data from the silicates and mixed silicates categories are included to provide an indication of the mineral phases measured. The box edges indicate the 25th and 75th percentiles, and the cross and the horizontal line dissecting the boxes represent the mean and median values respectively. The outliers extend to the 10 and 90 % thresholds of the data.

ACPD
15, 29403–29453, 2015

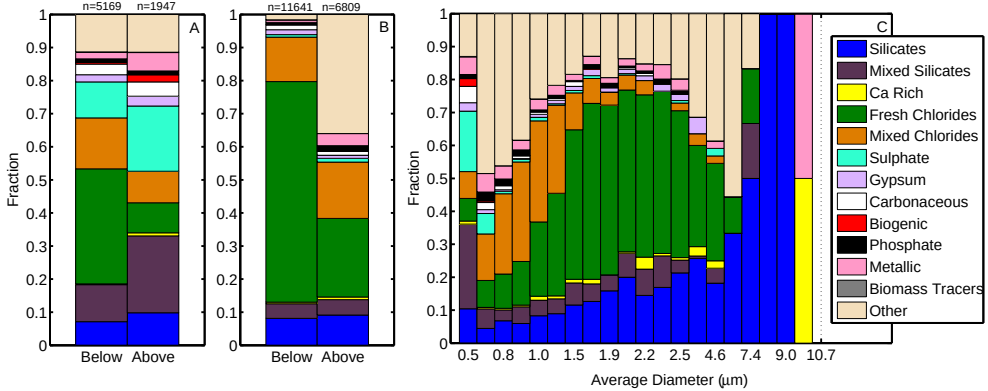

Figure 8. Compositional comparison between the below and above cloud samples from flight B764. Panel **(a)**: averaged particle classifications $\leq 0.5\,\mu m$; panel **(b)**: averaged particle classifications $>0.5\,\mu m$; panel **(c)**: Size-segregated classifications from the above cloud exposure. Each bin is normalised to show the fraction (by number) occupied by each classification, and the number of particles analysed are listed in panels **(a)** and **(b)**. The sizes indicated in panel **(c)** are the bin centres.

ACPD
15, 29403–29453, 2015

Table 1. Details of FAAM flights undertaken during the spring segment of the ACCACIA campaign which had viable filter exposures.

Flight number	Date (2013)	Flight region with respect to Svalbard
B760	21 Mar	South-East
B761	22 Mar	South-East
B762	23 Mar	South-East
B764	29 Mar	South-East
B765	30 Mar	South
B768	3 Apr	North-West

ACPD
15, 29403–29453, 2015

Table 2. Summary of sampling conditions during each filter exposure. The geographic positions are also listed. Values quoted are averaged quantities, with 1σ in brackets where appropriate.

Flight Number	Conditions sampled	Exposure Length (s)	Volume of Air (sL)	Latitude (°N)	Longitude (°E)	Altitude (m)
B760	Clear	600	2312.3[b]	76.2	24.5	102 (5)
B761	Clear[a]	1700	2608.4	76.4	26.5	238 (107)
B762	Cloud haze	660	826.4	76.8	28.0	375 (5)
B764	Clear[a]	540	754.8	76.6	27.2	91 (86)
B765	Clear	961	1249.3	76.2	22.0	71 (18)
B768	Clear	240	272.7	79.9	2.8	98 (44)

[a] Filter was collected mostly under clear conditions, although some in-cloud sampling was encountered at the end of the exposure.

[b] The total volume of air sampled by B760 is high given its exposure length due to higher-than-average flow rates applied during that flight.

ACPD
15, 29403–29453, 2015

Table 3. Main parameters applied with ESEM and EDAX™ Genesis software to carry out analysis of the ACCACIA aircraft filters.

ESEM/EDAX™ Genesis Analysis Parameters		
Beam voltage (kV)	15	
Working distance (mm)	10	
Operating current (µA)	~ 200	
Beam spot size	4	
Image resolution (px)	1024 × 800	
Particle coverage	70 %	
Total number of particles	135 364	
Magnifications applied	4000×	1000×
Filters analysed	1 and 10 µm	10 µm
Min. particle size (µm)	0.13	0.52
Field sizes (mm)	0.059 × 0.046	0.237 × 0.185

ACPD
15, 29403–29453, 2015

Table 4. Summary of the classification scheme adopted in this study.

Particle Class	Classification Criteria
Carbonaceous	Low counts, or zero, in all elements except C and O
Biogenic	Similar to carbonaceous; minor traces of K, P, S, Cl, Ca and/or Zn
Fresh Chlorides	Significant Na and Cl; low S and/or minor Ca fractions
Mixed Chlorides	Major fractions of Na, Cl, S; minor Ca and/or metallic fractions
Sulphates	Major S and Na and/or K fractions
Gypsum	Significant Ca and S
Ca-Rich	Significant Ca, with minor S or Mg
Silicates	Mixtures primarily containing Si and Al; variable Ca, Mg, Na, Fe and/or K components
Mixed Silicates	Similar to silicates; additional S and/or Cl component
Phosphates	Large P fraction
Metallic	Major fractions of Fe, Ti, Cr, Cu or Zn; also includes particles with high Al/negligible Si
Biomass Tracers	Dominant in K
Other	Particles not classified by these criteria

ACPD
15, 29403–29453, 2015

Table 5. Summary of sampling conditions during the two B764 exposures. Values quoted are averaged quantities, with 1σ in brackets where appropriate.

Case	Conditions sampled	Exposure Length (s)	Volume of Air (sL)	Latitude (°N)	Longitude (°E)	Altitude (m)
Below cloud	Clear*	540	754.8	76.6	27.2	91 (86)
Above cloud	Clear	720	1080.2	76.4	27.1	833 (59)

* Some cloud base sampling was encountered at the end of the exposure.

ACPD
15, 29403–29453, 2015